Evidence for a Bose-Einstein condensate of excitons

Mathieu Alloing[1], Mussie Beian[1], David Fuster[2], Yolanda González[2], Luisa González[2], Roland Combescot[3,4], Monique Combescot[5] and François Dubin[1]

[1] ICFO-The Institute of Photonic Sciences, Av. Carl Friedrich Gauss, num. 3, 08860 Castelldefels (Barcelona), Spain

[2] IMM-Instituto de Microelectrónica de Madrid (CNM-CSIC) Isaac Newton 8, PTM, E-28760 Tres Cantos, Madrid, Spain

[3] Laboratoire de Physique Statistique, Ecole Normale Supérieure UPMC Paris 06, Université Paris Diderot, CNRS, 24 rue Lhomond, 75005 Paris, France

[4] Institut Universitaire de France, 103 boulevard Saint-Michel, 75005 Paris, France

[5]Institut des Nanosciences de Paris, UPMC Paris 06, CNRS, 2 pl. Jussieu, 75005 Paris, France

April 16, 2013

Bose-Einstein condensation in dilute systems is a fascinating quantum phenomenon and its experimental observation in ultracold atomic vapors a milestone. Here, we report on experimental evidence for its occurrence in a gas of semiconductor excitons. The internal degrees of freedom of these subtle bosons plays a major role in their condensation. Indeed, excitons exist in two bright and two dark states. Dark excitons having the lowest energy, the Bose-Einstein condensate of excitons is a priori dark, i.e. not coupled to light. However, above a density threshold, carrier exchanges between bright and dark excitons bring a bright component to the condensate which becomes "gray" and can be studied through its bright part. Below a few Kelvin, our experiments display the very weak emission of spatially coherent and linearly polarized light expected for such a "gray" condensate which hides a

large exciton density in its dark component.

Bose-Einstein condensation of semiconductor excitons has received a considerable attention since its theoretical prediction in the 1960's [1–4]. In contrast with ^{4}He where superfluidity occurs in a strongly interacting liquid, Bose-Einstein condensation of excitons is expected to occur in a dilute gas. This makes it much closer to Einstein's original idea for non-interacting bosons. Excitons were even considered for a long time as the most promising candidates to demonstrate this remarkable quantum phase transition [5]. Indeed, excitons are very light bosonic particles compared to atoms; so, their quantum degeneracy should occur below a few degrees Kelvin [6], or even higher. Nevertheless, gaseous Bose-Einstein condensation has first been observed in ultracold atomic vapors at temperatures of the order of one micro-Kelvin [7].

In contrast with most commonly studied bosonic atoms, the exciton composite nature plays a key role in their condensation. In narrow quantum wells, excitons are made of one spin ($\pm 1/2$) electron and one "spin" ($\pm 3/2$) hole. These mainly interact through intraband Coulomb processes. However, weak interband valence-conduction Coulomb scatterings also exist, but only for excitons with total spin (± 1) made of ($\pm 3/2$) holes and ($\mp 1/2$) electrons. These repulsive processes bring the energy of (± 1) bright excitons, i.e., excitons coupled to $\sigma^{\pm}$ photons, above the one of "dark" excitons with total spin (± 2) made of ($\pm 3/2$) holes and ($\pm 1/2$) electrons. As a result, Bose-Einstein condensation of excitons must occur among the low energy dark states [8]. This feature, which makes exciton condensation definitely hard to evidence experimentally, could be the reason why unambiguous signatures of bright exciton condensates have not been given yet, despite several decades of experimental research. By contrast, the excitonic component of a polariton being by construction coupled to light, Bose-Einstein condensation of polaritons can be studied through photoluminescence and recently led to remarkable experiments [9–12].

To enter the regime in which excitons can undergo Bose-Einstein condensation, two main constraints must be fulfilled. First, exciton-exciton interactions have to be repulsive in order to prevent the

formation of biexcitons at densities where Bose statistics becomes dominant ($n_c \simeq m_X k_B T/\hbar^2 \sim 10^{10}$ cm^{-2} at 1 K, m_X being the exciton mass). In addition, excitons need to be long lived and efficiently cooled by the crystal lattice to build up a dense but cold ensemble. Here, we study electrically polarized (dipolar) excitons confined in a wide single quantum well which fulfill these constraints [13]. The electrical polarization keeps the electron and hole well apart, so that their wave functions have a small overlap leading to a long radiative lifetime. However, this overlap being not as small as for indirect excitons confiend in double quantum wells, dipolar excitons still exhibit a rather large energy splitting between bright and dark states (~ 20 μeV, see Ref. [14]).

Exploring the quantum regime, our experiments reveal the appearance of a very weak photoluminescence emission with macroscopic spatial coherence, the coherence length being ten times larger than the thermal wavelength. Strikingly, extended coherence is established in a region of the sample which darkens as the bath temperature is lowered but where the exciton gas is nevertheless as dense as in the brighest parts. This is a clear evidence for the formation of a nearly dark, or "gray", Bose-Einstein condensate, as theoretically predicted [15]. Indeed, if we merely had non-condensed excitons, the dark and bright exciton populations should be similar since their energy splitting ($\sim$20 μeV) is small compared to the thermal energy (~ 40 μeV at our lowest bath temperature). The dense but nearly dark exciton gas which is seen can only be explained by the formation of a dark condensate which captures most of the excitons, with a bright component [15] appearing in this condensate above a density threshold $\sim 10^9$ cm^{-2} – our estimated experimental exciton density ($\sim 10^{10}$ cm^{-2}) being above this threshold. Finally, the polarization of the observed weak photoemission is linear, in agreement with the predicted characteristics of a "gray" condensate [8, 15].

Our sample consists of a 25 nm wide GaAs quantum well embedded in a *n-i-n* field-effect device (Fig. 1.A). We bias a surface electrode to tune the density of electrons electrically injected in the quantum well while we control the hole density through a tightly focused (10 μm waist) laser excitation at 641.5 nm. By appropriately balancing these two creation processes, the ambipolar diffusion

of electrons and holes [16, 17], towards and outwards the illuminated region respectively, creates a ring of dipolar excitons ≈ 30 μm away from the laser excitation. As we lower the bath temperature T_b from 7K to 370 mK, the ring contracts and fragments into small beads (Fig. 1.B) while the exciton concentration increases, as seen from the photoluminescence emitted at the position of the ring which shifts by ≈ 1.5 meV towards higher energies (Fig. 1.C). This blue-shift, distinctive to dipolar excitons, reveals the increase of repulsive dipolar interactions with increasing exciton density. Following latest theoretical works [18, 19], we estimate that, for T_b=370 mK, the exciton density at the position of the ring reaches $\approx 10^{10}$ cm^{-2}.

To study the quantum nature of excitons formed in the region of the ring, we measured the first order spatial coherence $|g^{(1)}|$ of the photoluminescence [20], bright excitons having a fluorescence emission reflecting their wave function. Thus, we distinguish classical and quantum regimes by the degree of spatial coherence, the classical coherence length being of the order of the de Broglie wavelength ($\lambda_{dB} \sim 100$ nm at sub-Kelvin temperatures). In our experiments (Fig.1.A), we use a Mach-Zehnder interferometer to assess the coherence length of bright excitons. One arm of the interferometer displaces the photoluminescence laterally by δ_x with respect to the second arm; it also tilts it vertically, so that output interference fringes end up aligned horizontally [20, 21]. By scanning the phase of the interferometer, we reconstruct point by point the amplitude of the interference contrast and then infer the map of the emission first order spatial coherence from which we deduce the exciton coherence length ξ (see also supplementary informations).

Figure 2 shows $|g^{(1)}|$ for $\delta_x = 1.5\mu$m in the region where the ring is formed. At T_b= 7K, (Fig. 2.D), the interference contrast does not vary significantly; it is approximately equal to 10-15 % across the emission; so, $\xi \leq 200$ nm. Quite differently, at T_b= 370 mK (Fig. 2.C), the interference contrast exhibits a pattern correlated with the spatial profile of the photoemission (Fig. 2.A) but in a way which could be surprising at first. Indeed, Figure 3.A shows that the interference contrast is minimal ($\sim$10 %) in the bright part of the ring while, in the outer region (underlined by the contour lines in

Fig. 2.A), $|g^{(1)}|$ can reach ≈ 40 %, i.e., over half the auto-correlation value (70% for $\delta_x = 0$). This shows that, in the outer region which darkens as the bath temperature is lowered, bright excitons have a coherence length $\xi \sim 1.5$ μm, one order of magnitude larger than the de Broglie wavelength.

Strikingly, bright excitons exhibit a macroscopic spatial coherence *outside* the ring where the photoluminescence intensity is reduced by 10 to 20-fold compared to the bright parts of the ring where the intensity is maximum but the interference contrast low (Figs. 2.E and 3.A). By only considering this intensity difference, we would conclude that the concentration of bright excitons only is $\approx$ 10^8-10^9 cm^{-2} outside the ring, i.e., well below the critical density n_c to form a quantum gas with macroscopic spatial coherence ($n_c \sim 10^{10}$ cm^{-2} at 1K). Yet, the photoluminescence emitted at the position of the ring fragments and in the outer region are essentially identical (Fig. 1.C). Since the energy of emitted photons is governed by the exciton density [18, 19], regardless of the fact that these excitons are dark or bright, this shows that the total exciton density is the same outside and on the ring – by contrast with fragmentated rings observed with indirect excitons confined in double quantum wells for which dark regions emit a photoluminescence at a lower energy than bright regions [22, 23]. From the experiments shown in Fig.1.C and Fig.2, we are then led to conclude that, outside the bright ring, dark excitons build up a dense ensemble which undergoes a Bose-Einstein condensation when the bath temperature decreases. From the variation of the exciton coherence length, we estimate that non-classical correlations between excitons appear below a critical bath temperature of the order of 2-3K (Fig. 3.B). It is worth noting that the existence of condensed dark excitons outside the bright parts of the fragmented ring had already been suggested a few years ago [24].

In order to obtain further insight into the internal structure of the condensate, we filtered the polarization of the photoluminescence which should reflect this structure. Indeed, bright excitons with angular momenta (± 1) are responsible for the emission of ($\sigma^{\pm}$) polarized light. By contrast, dark excitons (± 2) are not coupled to light. However, recent theoretical works have underlined processes that can turn dark excitons into bright ones [15, 21, 25–27]. In particular, carrier exchanges between

excitons with opposite spins introduce a bright component into the dark exciton condensate above a critical density, making it turn "gray" with a linear polarization [15]. Figure 4.B shows that indeed the photoluminescence is linearly polarized in the outer region of the ring at T_b= 370 mK – the degree of circular polarization being not as significant (Fig.4.C). Interestingly, the inner region of the exciton ring also exhibits a linear polarization, but along the orthogonal direction. These observations contrast with recent studies performed in double quantum well heterostructures where indirect excitons exhibit correlated patterns of both linear and circular polarizations [21, 28]. These patterns have been interpreted in terms of coherent exciton transport and spin-orbit coupling. Our experiments, which do not reveal such phenomena, are performed in a single quantum well with an energy splitting between bright and dark excitons much larger than in bilayer heterostructures. Since this energy splitting plays a key role in selecting the specific condensate which is formed, it is reasonable to conclude that experiments performed in single and double quantum wells probe distinct regimes.

As a final remark, let us note that one might wonder if our essentially two-dimensional geometry would not dramatically affect Bose-Einstein condensation. However, this is not the case because condensation occurs in small regions. This stabilizes [7] Bose-Einstein condensation. Moreover phase fluctuations, which are responsible [7] for the main qualitative differences between 2D and 3D systems, are then quenched; so, the condensate should be fairly similar to a 3D condensate.

References and Notes

[1] S.A. Moskalenko, Fiz. Tverd. Tela (Leningrad) **4**, 276 (1962)

[2] J. M. Blatt et al., Phys. Rev. **126**, 1691 (1962)

[3] L.V. Keldysh and YuV. Kopaev, Sov. Phys. Solid State **6**, 2219 (1965)

[4] L.V. Keldysh and A.N. Kozlov, Sov. Phys. JETP **27**, 521 (1968)

[5] *"Bose-Einstein condensation"*, Eds. A. Griffin, D. W. Snoke, S. Stringari (Cambridge Univ. Press, 1995)

[6] *"Bose-Einstein Condensation of Excitons and Biexcitons"*, S.A. Moskalenko, D. W. Snoke, (Cambridge Univ. Press, 2000)

[7] *"Bose-Einstein Condensation"*, Lev. P. Pitaevskii, Sandro Stringari (Oxford university Press, 2003)

[8] M. Combescot, O. Betbeder-Matibet, R. Combescot, Phys. Rev. Lett. **99**, 176403 (2007)

[9] H. Deng et al., Science **298**, 199 (2002)

[10] J. Kasprzak et al., Nature **443**, 409 (2006)

[11] R. Balili et al., Science **316**, 1007 (2007)

[12] E. Wertz et al., Nat. Phys. **6**, 860864 (2010)

[13] V.B. Timofeev, A.V. Gorbunov, J. App. Phys. **101**, 081708 (2007)

[14] E. Blackwood et al., Phys. Rev. B **50**, 14246 (1994)

[15] R. Combescot, M. Combescot, Phys. Rev. Lett. **109**, 026401 (2012)

[16] L. V. Butov et al., Phys. Rev. Lett **92**, 117404 (2004)

[17] R. Rapaport et al., Phys. Rev. Lett **92**, 117405 (2004)

[18] C. Schindler and R. Zimmermann, Phys. Rev. B **78**, 045313 (2008)

[19] B. Laikhtman. and R. Rapaport, Phys. Rev. B **80**, 195313 (2009)

[20] see supplementary informations

[21] A.A. High et al., Nature **483**, 584 (2012)

[22] L. V. Butov, A. C. Gossard, D. S. Chemla, Nature **418**, 751(2002)

[23] S. Yang, A.V. Mintsev, A.T. Hammack, L.V. Butov, and A.C. Gossard, Phys. Rev. B **75**, 033311 (2007)

[24] M. Combescot, M.N. Leuenberger, Solid State Comm. **149**, 567 (2009)

[25] M. Ali Can and T. Hakioglu, Phys. Rev. Lett. **103**, 086404 (2009)

[26] M. Matuszewski et al., Phys. Rev. B **86**, 115321 (2012)

[27] D.V. Vishnevsky et al., arXiv:1212.5485 (2012)

[28] A.A. High, et al., arXiv:1302.3852 (2013)

Acknowledgments: This work was supported financially by the EU-ITN INDEX, by the Spanish MEC (TOQATA), by the Spanish MINECO (Grant TEC2011-29120-C05-04), CAM (Grant S2009ESP-1503) and by the ERC AdG QUAGATUA. F.D. also acknowledges the Ramon y Cajal program. Furthermore M.A. and F.D. are grateful to M. Lewenstein for his continuous support.

Author Information: The authors declare no competing financial interests.

Correspondence should be sent to F.D. (francois.dubin@icfo.es).

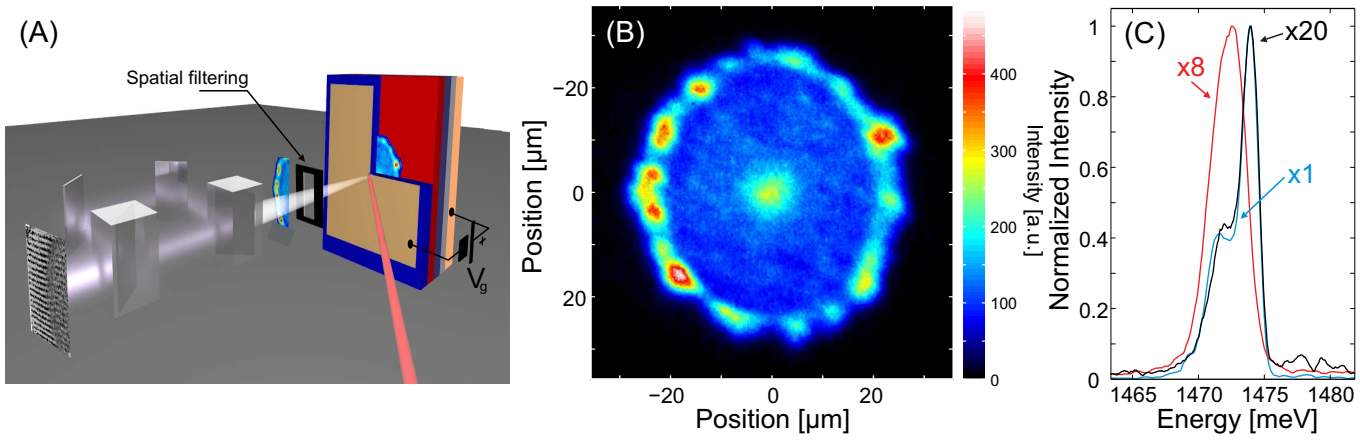

Fig. 1. (A): Field-effect device and Mach-Zehnder interferometer used in our experiments. (B): Fragmented exciton ring at T_b= 370 mK. (C): Rescaled photoluminescence spectra emitted at the position of the ring at 7 K (red), 370 mK (blue), and 7 μm outside the ring at 370 mK (black). The last two spectral profiles are essentially identical besides a factor of 20 in the intensity. Here as well as in the other figures, measurements are made in a 40ns long time interval, 10 ns after extinction of a 1 μs laser excitation.

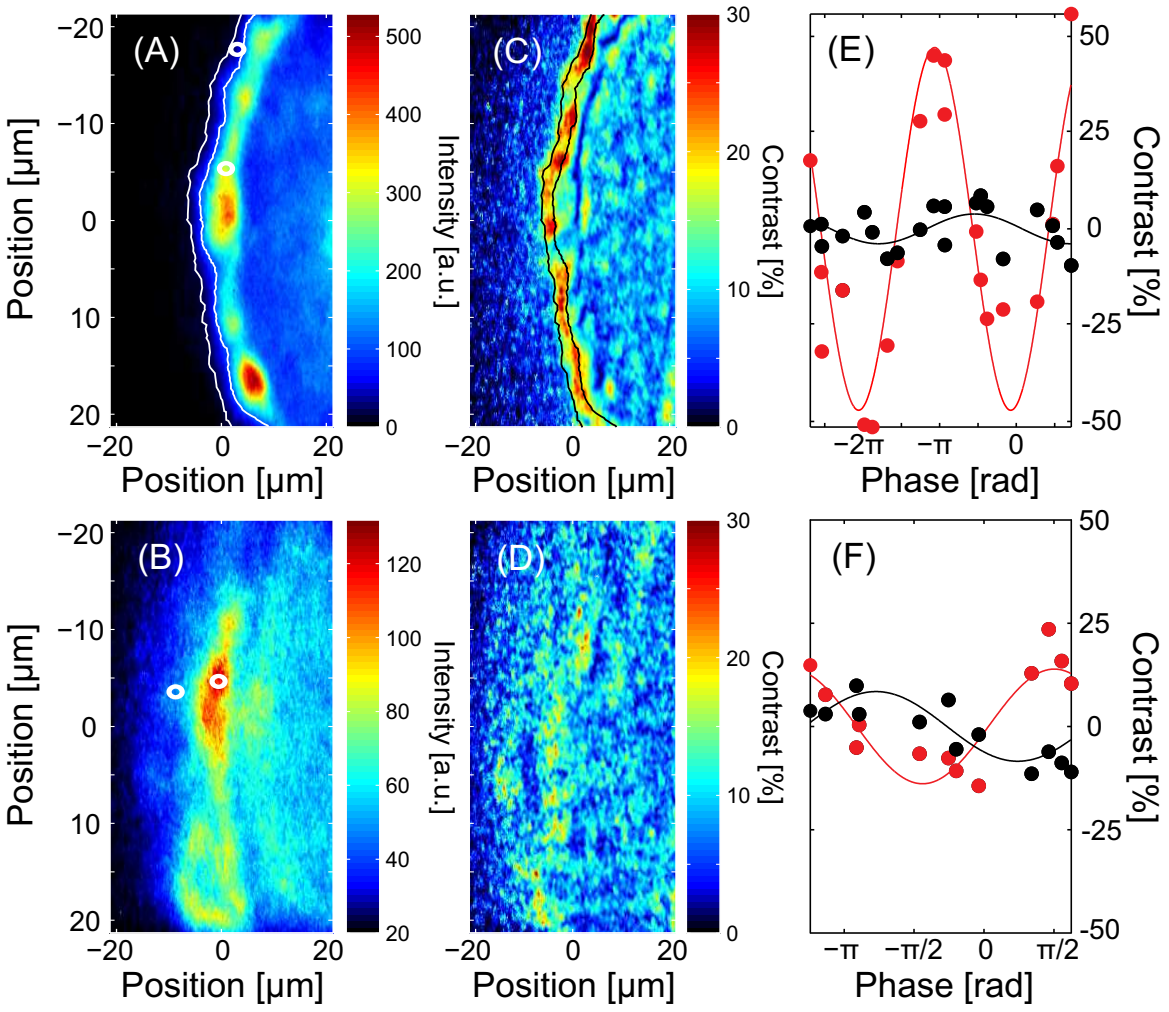

Fig. 2. (A-B): Photoluminescence from the same position of the ring at 370 mK (A) and 7K (B). A large fraction of the image darkens as the bath temperature decreases. (C-D): Map of the interference contrast for δ_x=1.5 μm at 370 mK (C) and 7K (D). The two contour lines in (A) and (C) outline the same dark outer region where the excitons coherence length is macroscopic. (E-F): Variation of the interference signal at 370 mK (E) and 7 K (F), as a function of phase of the interferometer. Data are taken at the position of the ring (black) and 5 μm outside the ring (red). The white circles in (A) and (B) show these positions.

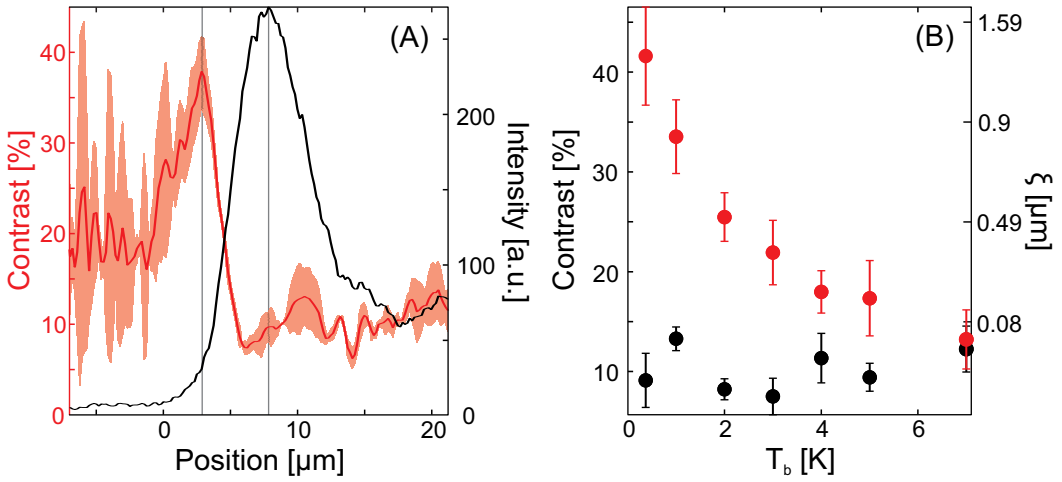

Fig. 3. (A): Intensity (dark) and interference contrast (red) of the photoemission across the fragmentated ring at 370 mK. The red area shows the relative error in our measurements. The vertical lines underline the maximum of the emission, i.e. the position of the ring, and the maximum of the interference contrast where the intensity is reduced by 10-fold. (B): Interference contrast for δ_x=1.5 μm and the corresponding coherence length ξ as a function of the bath temperature T_b, taken 5 μm outside the ring (red) and at the position of the ring (black). Non-classical coherence builds-up in the "gray" part of the ring below a few degrees Kelvin.

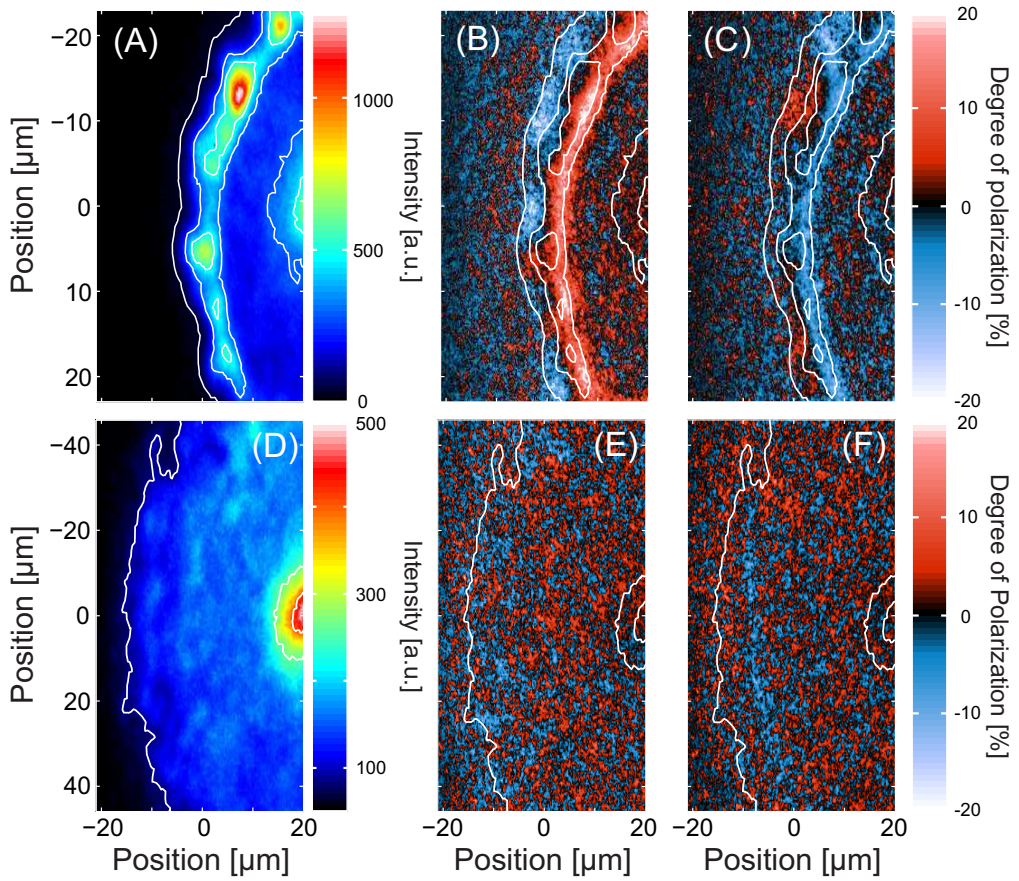

Fig. 4. Exciton ring at 370 mK (A) and 4K (D). (B)-(E): Patterns of linear polarizations at 370 mK (B) and 4K (E). The blue and red color are associated to orthogonal polarizations. (C)-(F): Patterns of circular polarizations at 370 mK (C) and 4K (F). The blue and red color are now associated to σ^+ and σ^- polarized light respectively. In (B) we observe that the photoemission is mostly linearly polarized in the outer region which darkens when the bath temperature decreases and where extended spatial coherence is also observed.

Supplementary Informations:

First order coherence of the photoluminescence

To quantify the first order coherence of dipolar excitons, we magnify and spatially filter the photoluminescence emitted in the region of the ring. This part of the emission is directed towards a Mach-Zehnder interferometer with a path length difference between its two arms that is actively stabilized. Thus, we control the phase ϕ of output interference signals with a $\approx (\pi/10)$ accuracy. The magnified photoluminescence is then split between the arms 1 and 2 of the interferometer, and we introduced a vertical tilt angle (α) between the output of the two arms. Hence, interference fringes are aligned horizontally [1, 2], α being set such that the interference period is ≈ 4 μm. In this situation, the outputs produced by two arms are laterally shifted, by δ_x, while the path length difference remains close to zero. This allows us to derive the degree of spatial coherence of the bright excitons.

The output of our interferometer, I_{12}, can be modelled as

$$I_{12}(\mathbf{r};\delta_x) = \langle|\psi_0(\mathbf{r},t) + e^{i(q_\alpha y+\phi)}\psi_0(\mathbf{r}+\delta_x,t)|^2\rangle_t,$$

where $\psi_0(\mathbf{r})$ is the photoluminescence field which reflects the bright excitons wave function, $\langle..\rangle_t$ denotes the time averaging , $\mathbf{r}$=(x,y) is the coordinate in the plane of the quantum well while $q_\alpha = 2\pi\sin(\alpha)/\lambda$ with λ equal to the emission wavelength. By recording individually the output of the two arms, I_1 and I_2, we can compute interferograms or normalized interference patterns $I_{int}=(I_{12}-I_1-I_2)/2\sqrt{I_1 I_2}$ which reveal the first order coherence function of indirect excitons,

$$g^{(1)}(\mathbf{r};\delta x) = \frac{\langle\psi_0^*(\mathbf{r},t)\psi_0(\mathbf{r}+\delta_x,t)\rangle_t}{(\langle|\psi_0(\mathbf{r},t)|^2\rangle_t\langle|\psi_0(\ \mathbf{r}\ +\delta_x,t)|^2\rangle_t)^{1/2}}.$$

Indeed, we have $I_{int}(\mathbf{r};\delta_x)=\cos(q_\alpha y+\phi+\phi_\mathbf{r})|g^{(1)}(\mathbf{r};\delta x)|$ where $\phi_\mathbf{r}=\arg(g^{(1)})$. Hence, normalized interferences have a visibility controlled by the degree of spatial coherence of bright excitons, while the position of the interference fringes reveals the phase of the $g^{(1)}$-function, i.e., the phase difference

between the interfering excitonic wave functions.

In Figure S1, we present some interferograms which we used to study the spatial coherence of dipolar excitons (Figure 2). Varying the phase of the interferomer, ϕ, we deduce $|g^{(1)}(\mathbf{r};\delta_x)|$ as shown in Figure 2.C-D.

Our experiments emphasize regions where the intensity of the photoluminescence is weak while the degree of spatial coherence is large. To quantify it, we used standard numerical routines to fit the variation of I_{int} as a function of ϕ. Following this approach, we noted that the fitting error becomes large when the intensity of the photoluminescence emission reaches 1% of its maximum at the position of the ring. This corresponds to $\approx$ 10-20 counts on our photo-detector. This limitation is illustrated in Figure S2 which presents the map of the interference contrast together with its relative error for the experiment shown in Figure 2.C. There, we verify that the interference contrast is large and measured with a good precision in the outer region of the ring while for lower intensities the fitting error is of the same order as the contrast we extract. To produce "simple" maps of the photoluminescence spatial coherence (Figure 2.C-D), we discard the regions where the fitting error is large. For that, we damp the value of the interference contrast by imposing an exponential decay for the points where the photoluminescence intensity is low; precisely, we set the decay at 20 counts. This yields to the results shown in Figure 2.C-D.

Finally, to extract quantitatively the bright excitons coherence length ξ, we model the variation of $|g^{(1)}|$ by the convolution between a Gaussian profile with a 1.5 μm full-width at half-maximum and an exponential decay [3, 4]. The former function accounts for our instrumental resolution while the latter function provides the theoretical variation of the $g^{(1)}$-function ($|g^{(1)}(\delta_x)| \propto e^{-\delta x/\xi}$). For our interferometric setup, we calibrated the variation of $|g^{(1)}|$ as a function δ_x in previous experiments [2]. Thus, we retrieve the coherence length of bright excitons (ξ) from the interference contrast at δ_x=1.5 μm (Figure 2.H).

Sample structure

We studied a 1 μm thick n^+-i-n^+ field-effect device where a 250 Å wide GaAs quantum well is embedded. The quantum well is surrounded by $Al_{0.3}Ga_{0.7}As$ barriers incorporating a ten-period (2/2 nm) GaAs/$Al_{0.3}Ga_{0.7}As$ superlattice. The quantum well is placed 900 nm below a millimeter wide semi-transparent gate electrode deposited on the surface of the sample. For our measurements this electrode was biased at a constant voltage V_g=-4.7 V with respect to the conductive sample's substrate that was grounded.

References and Notes

[1] A.A. High et al., Nature **483**, 584 (2012)

[2] M. Alloing, D. Fuster, Y. Gonzalez, L. Gonzalez and F. Dubin, arXiv:1210.3176

[3] M.M. Fogler et al., Phys. Rev. B **78**, 035411 (2008)

[4] D. Semkat et al., Nano Lett. **12**, 5055 (2012)

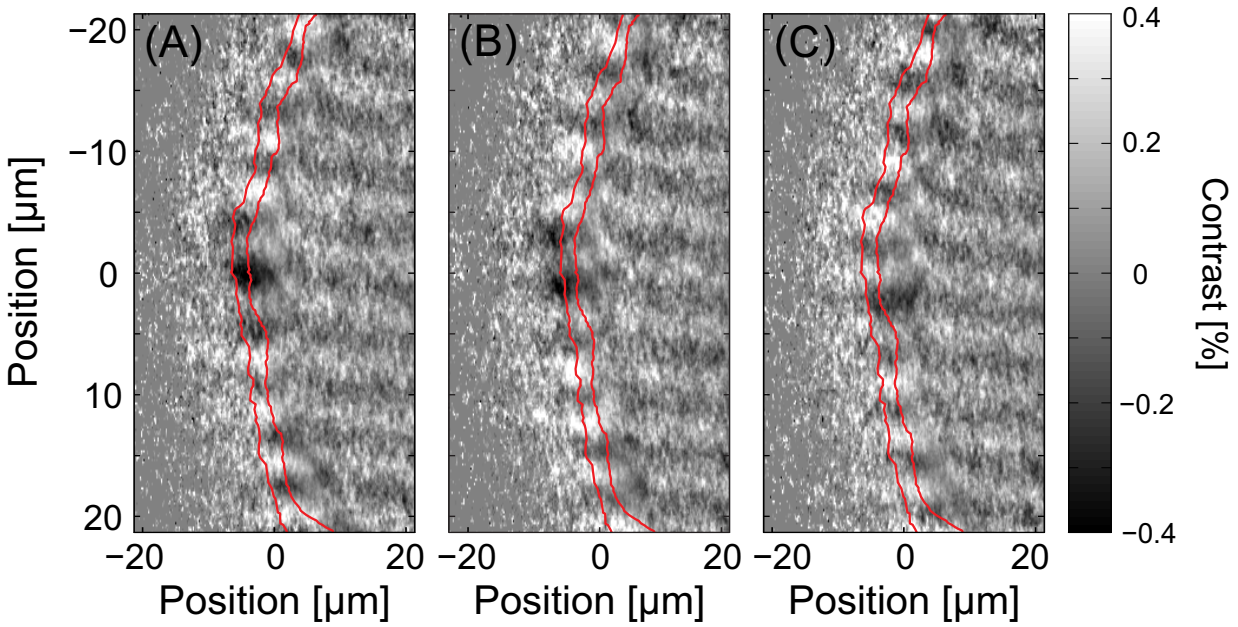

Fig. S1. (A-C): Normalized interference patterns I_{int} obtained for δ_x= 1.5 μm. From (A) to (C) the phase of the interferometer ϕ are 0, $\pi/2$, and π. From such interferograms, we computed the map of $|g^{(1)}|$ shown in Figure 2.C, the two red lines underlining the region where spatial coherence is macroscopic, as in Fig.2.A and 2.C. All the measurements have been realized by integrating in a 40 ns long time interval 10 ns after extinction of a 1 μs laser excitation at 370 mK.

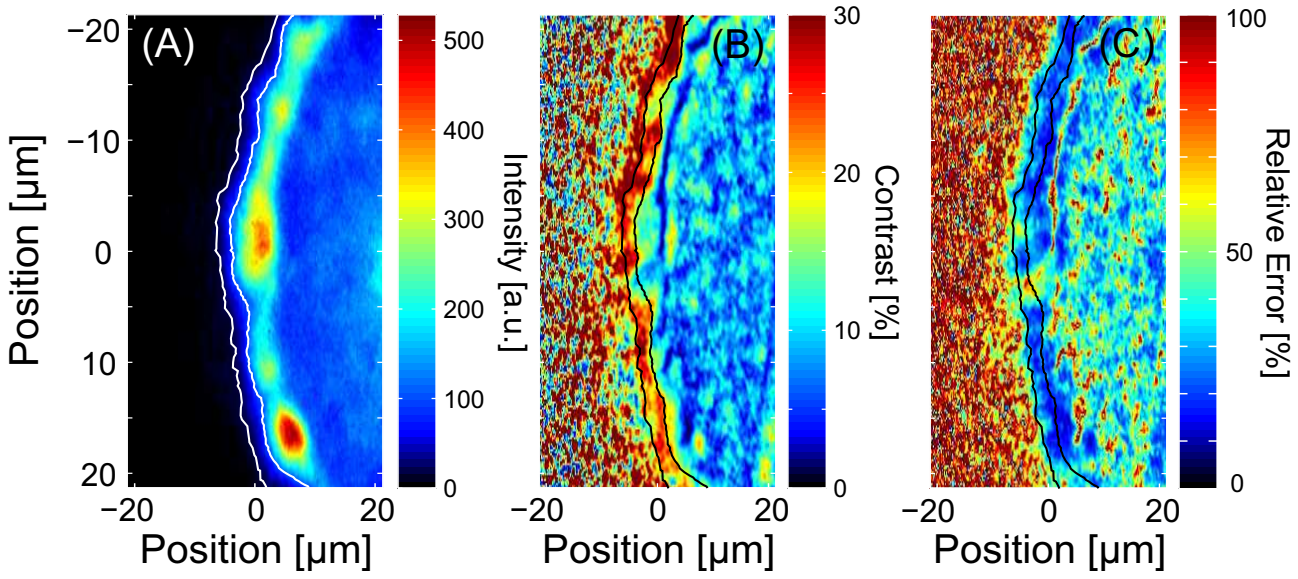

Fig. S2. (A): Photoluminescence emission in the region of the fragmented ring at 370 mK. This image is identical to the one shown in Fig.2.A. (B): Map of the interference contrast that we obtain by fitting point by point the variation of the interference signal as a function of ϕ. The relative error of the fit is displayed in (C) which shows that we can not extract the contrast with a sufficient accuracy for regions where the photoluminescence intensity is less than ≈ 20 counts. In (A-C) the two contour lines show the outer part of the ring where we resolve, in a clear way, macroscopic spatial coherence, as shown in Figure 2.C.